Synthesis of Iron Nanoparticles via Chemical Reduction with Palladium Ion Seeds

Kuo-Cheng Huang[†,‡] and Sheryl H. Ehrman*[,†]

Department of Chemical and Biomolecular Engineering, University of Maryland, College Park, Maryland 20742, and Department of Chemical Engineering, National Tsing-Hua University, Hsinchu, Taiwan 300

Received June 26, 2006. In Final Form: October 18, 2006

We report on the synthesis of highly monodisperse iron nanoparticles, using a chemical reduction method. Iron nanoparticles with an average diameter of 6 nm and a geometric standard deviation of 1.3 were synthesized at a pH of 9.50 from ferric chloride precursor with sodium borohydride as the reducing agent, polyacrylic acid as the dispersing agent, and palladium ions as seeds for iron nanoparticle nucleation. The resulting nanoparticles were ferromagnetic at 5 K and superparamagnetic at 350 K. The dispersing agent polyacrylic acid (PAA) was shown to prevent iron nanoparticles and possibly palladium clusters from aggregating; in the absence of PAA, only aggregated iron nanoparticles were obtained. The addition of palladium ions decreased the diameter of iron nanoparticles presumably by providing sites for heterogeneous nucleation onto palladium clusters. In the absence of palladium ions, the mean diameter of iron nanoparticles was approximately 110 nm and the standard deviation increased to 2.0. The pH of the solution also was found to have a significant effect on the particle diameter, likely by affecting PAA ionization and altering the conformation of the polymer chains. At lower pH (8.75), the PAA is less ionized and its ability to disperse palladium clusters is reduced, so the number of palladium seeds decreases. Therefore, the resulting iron nanoparticles were larger, 59 nm in diameter, versus 6 nm for nanoparticles formed at a pH of 9.50.

Introduction

Iron is one of the most abundant and widely used elements on earth. Iron nanoparticles have a huge potential for different applications including magnetic fluids,[1] catalysts for carbon nanotube formation,[2] magnetic resonance imaging (MRI) contrast agents,[3,4] nickel−iron batteries, and catalysts and sorbents for environmental remediation.[5,6] Depending on the application, different forms of iron nanoparticles are needed. For example, for Ni−Fe batteries and environmental remediation, nanosized aggregated iron powder is suitable. However, well-dispersed colloidal iron is required for applications in biological systems such as MRI contrast enhancement and biomaterials separation. In another important application, carbon nanotubes can be grown on silicon by chemical vapor deposition (CVD) using iron, cobalt, or nickel nanoparticles as the catalysts. To prevent interference between nanotubes, especially in the application of field-emission sources, dispersive separation of nanoparticles on the substrate is very important.[7] Spin-coating is an economical and convenient method to disperse the nanoparticles on the substrate over a large area,[8] and for this, a suspension of unagglomerated iron nanoparticles is needed.

Many chemical synthesis methods for iron nanoparticles have been reported in the literature. Two important synthesis routes are the thermal decomposition[9−15] and the chemical reduction.[5,16−21] methods. In the thermal decomposition method, iron pentacarbonyl ($Fe(CO)_5$) is dissolved in an organic solvent such as octyl ether and then heated to near 200 °C. An organic surfactant such

* To whom correspondence should be addressed. E-mail: sehrman@eng.umd.edu. Phone: (301) 405-1917. Fax: (301) 405-0523.

† University of Maryland.

‡ National Tsing-Hua University.

(1) Wu, K. T.; Yao, Y. D.; Wang, C. R. C.; Chen, P. F.; Yeh, E. T. Magnetic field induced optical transmission study in an iron nanoparticle ferrofluid. *J. Appl. Phys.* **1999**, *85* (8), 5959−5961.

(2) Wong, E. W.; Bronikowski, M. J.; Hoenk, M. E.; Kowalczyk, R. S.; Hunt, B. D. Submicron patterning of iron nanoparticle monolayers for carbon nanotube growth. *Chem. Mater.* **2005**, *17* (2), 237−241.

(3) Jun, Y. W.; Huh, Y. M.; Choi, J. S.; Lee, J. H.; Song, H. T.; Kim, S.; Yoon, S.; Kim, K. S.; Shin, J. S.; Suh, J. S.; Cheon, J. Nanoscale size effect of magnetic nanocrystals and their utilization for cancer diagnosis via magnetic resonance imaging. *J. Am. Chem. Soc.* **2005**, *127* (16), 5732−5733.

(4) Mornet, S.; Vasseur, S.; Grasset, F.; Duguet, E. Magnetic nanoparticle design for medical diagnosis and therapy. *J. Mater. Chem.* **2004**, *14* (14), 2161−2175.

(5) Li, F.; Vipulanandan, C.; Mohanty, K. K. Microemulsion and solution approaches to nanoparticle iron production for degradation of trichloroethylene. *Colloids Surf., A* **2003**, *223* (1−3), 103−112.

(6) Zhang, W. X. Nanoscale iron particles for environmental remediation: An overview. *J. Nanopart. Res.* **2003**, *5* (3−4), 323−332.

(7) Teo, K. B. K.; Chhowalla, M.; Amaratunga, G. A. J.; Milne, W. I.; Hasko, D. G.; Pirio, G.; Legagneux, P.; Wyczisk, F.; Pribat, D. Uniform patterned growth of carbon nanotubes without surface carbon. *Appl. Phys. Lett.* **2001**, *79* (10), 1534−1536.

(8) Cho, Y. S.; Choi, G. S.; Hong, S. Y.; Kim, D. Carbon nanotube synthesis using a magnetic fluid via thermal chemical vapor deposition. *J. Cryst. Growth* **2002**, *243* (1), 224−229.

(9) Chen, M.; Yamamuro, S.; Farrell, D.; Majetich, S. A. Gold-coated iron nanoparticles for biomedical applications. *J. Appl. Phys.* **2003**, *93* (102), 7551.

(10) Farrell, D.; Majetich, S. A.; Wilcoxon, J. P. Preparation and characterization of monodisperse Fe nanoparticles. *J. Phys. Chem. B* **2003**, *107* (40), 11022.

(11) Huber, D. L.; Venturini, E. L.; Martin, J. E.; Provencio, P. P.; Patel, R. J. Synthesis of highly magnetic iron nanoparticles suitable for field structuring using a beta-diketone surfactant. *J. Magn. Magn. Mater.* **2004**, *278* (3), 311.

(12) Hyeon, T.; Su, Seong, L.; Park, J.; Chung, Y.; Hyon, Bin, N. Synthesis of highly crystalline and monodisperse maghemite nanocrystallites without a size-selection process. *J. Am. Chem. Soc.* **2001**, *123* (51), 12798.

(13) Kang, E.; Park, J.; Hwang, Y.; Kang, M.; Park, J.-G.; Hyeon, T. Direct synthesis of highly crystalline and monodisperse manganese ferrite nanocrystals. *J. Phys. Chem. B* **2004**, *108* (37), 13932.

(14) Nikitenko, S.; Koltypin, Y.; Gedanken, A.; Markovich, V.; Rosenberg, E.; Gorodetsky, G. *Synthesis of air-stable iron-iron carbide nanocrystalline particles showing very high saturation magnetization*; Institute of Electrical and Electronics Engineers Inc.: Amsterdam, The Netherlands, 2002; p 2.

(15) Xu, X. L.; Friedman, G.; Humfeld, K. D.; Majetich, S. A.; Asher, S. A. Synthesis and utilization of monodisperse superparamagnetic colloidal particles for magnetically controllable photonic crystals. *Chem. Mater.* **2002**, *14* (3), 1249−1256.

(16) Glavee, G. N.; Klabunde, K. J.; Sorensen, C. M.; Hadjipanayis, G. C. Chemistry of Borohydride Reduction of Iron(II) and Iron(III) Ions in Aqueous and Nonaqueous Media. Formation of Nanoscale Fe, FeB, and Fe2B Powders. *Inorg. Chem.* **1995**, *34* (1), 28−35.

(17) Lim, S. K.; Chung, K. J.; Kim, Y.-H.; Kim, C. K.; Yoon, C. S. Synthesis of iron oxide nanoparticles in a polyimide matrix. *J. Colloid Interface Sci.* **2004**, *273* (2), 517.

10.1021/la0618364 CCC: $37.00
Published on Web 12/09/2006

as oleic acid or oleylamine is used to prevent the iron nanoparticles from aggregation and agglomeration. By this method, small and uniform iron nanoparticles with high purity can be manufactured. However, it is an uneconomical process because elevated temperatures and expensive highly toxic precursors are needed. As a result, materials made by this route are not suitable for applications requiring large quantities of iron nanoparticles, such as environmental remediation or nickel−iron batteries. In addition, requirement of an organic solvent such as octyl ether makes this method unfavorable for biological applications.

Compared to thermal decomposition, the chemical reduction method is economical and may potentially lead to more biocompatible particles. In the chemical reduction process, an iron salt such as ferric chloride ($FeCl_3$) is reduced in aqueous solution to form iron nanoparticles. Hydrazine hydrate ($N_2H_4 \cdot H_2O$) and sodium borohydride ($NaBH_4$) are the most frequently used reducing agents.[19−21] Hydrazine hydrate is added to alkaline solutions, and sodium borohydride is suitable for neutral or acid solutions. Iron nanoparticles usually can be obtained without use of dispersing agents such as surfactants or water-soluble polymers. However, to prevent aggregation and agglomeration, dispersing agents can be added to establish steric barriers between iron nanoparticles.

In this work, iron nanoparticles were synthesized by a chemical reduction method from iron chloride hydrate. Sodium borohydride was used as the reducing agent. To obtain small particles and to promote formation of metallic iron instead of iron oxide, a trace amount of palladium ion was added to promote nucleation of iron nanoparticles. Iron, like other base metals such as nickel and cobalt, is difficult to reduce compared to noble metals because of its high standard reduction potential. As a result, in the case of nickel, addition of a trace amount of noble metal ion has been shown to promote nickel nanoparticle nucleation in both the thermal decomposition and chemical reduction synthesis routes.[22,23] Noble metal ion seeds have also recently been used to achieve shape control of PdSe nanoparticles.[24] To the best of our knowledge, there is no similar report on adding noble metal nuclei in the iron nanoparticle system. In addition, several kinds of dispersing agents were studied to evaluate their capability to prevent iron nanoparticles from aggregating. Here, it is shown that, by adjusting and controlling these process parameters such as the presence/absence of seed material, dispersing agent, and pH, iron nanoparticles in several size ranges can be obtained for use in a variety of applications.

Experimental Section

Synthesis of Iron Nanoparticles without Dispersing Agent. The reaction to form nanoparticles was carried out by mixing two solutions, called here solution A and solution B. For solution A, 1.35 g of ferric chloride hydrate ($FeCl_3 \cdot 6H_2O$; Fisher) was dissolved in 40 mL of deionized water. For solution B, 0.95 g of sodium borohydride ($NaBH_4$; 98%, Acros) was dissolved in 10 mL of deionized water. Solution A was then added to solution B dropwise under vigorous stirring. Black powder was produced in less than 1 s after addition of solution A to solution B. After reaction, the product particles were separated from the solution by a strong magnet and washed with deionized water. Freeze-drying overnight was utilized to dry the particles.

To study the seeding effect of palladium, 0.5 mL of $PdCl_2$ (99%, Sigma) solution (0.01 M) was added to solution A before it was mixed with solution B, and then the same procedures mentioned above were followed. This $PdCl_2$ solution was prepared from 0.1615 g of palladium chloride dissolved in 91 mL of 0.1 M HCl. The final mole ratio of Pd to Fe was 1:1000.

Synthesis of Iron Nanoparticles with Dispersing Agent at Lower pH. To prevent the iron nanoparticles from agglomerating, dispersing agents were added during synthesis. Several commonly used dispersing agents were evaluated in this work including poly(vinylpyrrolidone) (PVP; average molecular weight 10000, Sigma), poly(acrylic acid) (PAA) solution (35%, Aldrich), carboxymethylcellulose sodium salt (CMC; low viscosity, Fluka), and sodium dodecylbenzenesulfonate (SDS; 80%, Sigma). Of these, PAA was found to disperse iron nanoparticles well. Other polymers and surfactants such as PVP, CMC, and SDS resulted in agglomeration of nanoparticles, which settled immediately from solution.

The details of the experiments with the other dispersing agents are given in the Supporting Information, and the procedure for use of PAA is as follows. The original concentration of PAA solution as purchased was 35 wt %. It was then diluted from 35 to 3.5 wt % by adding deionized water. The synthesis was performed by mixing two solutions, called here solution C and solution D. For solution C, 0.27 g of ferric chloride hydrate was dissolved in 20 mL of deionized water and then mixed with 20 mL of PAA solution (3.5 wt %). When mixed, the color of the ferric chloride solution turned from yellow to orange. For solution D, 0.75 g of sodium borohydride was dissolved in 10 mL of deionized water. Solution D was then added to solution C dropwise under vigorous stirring. Gradually, with addition of solution D, the solution became darker and eventually became completely black. The reaction was accompanied by generation of numerous bubbles. The reaction was presumed to be complete once bubble formation ceased. To separate the iron nanoparticles, a strong magnet was used. The iron nanoparticles were washed, redispersed in deionized water, and freeze-dried overnight.

As in the synthesis of iron nanoparticles without dispersing agent, the seeding effect of palladium was also investigated in this work. These experiments followed the same procedures mentioned above except 0.1 mL of palladium chloride solution (0.01 M) was added to solution C before it was mixed with solution D. The final Pd to Fe mole ratio was 1:1000, and the final pH value of the solution was 8.75. Assuming a density of 1 g cm^{-3} for PAA, the weight ratio of Fe to PAA in the final solution was 1:14.

Synthesis of Iron Nanoparticles with Dispersing Agent at Higher pH. Similar to the synthesis process of iron nanoparticles with dispersing agent at low pH, the reaction was performed by mixing of two solutions called solution E and solution F. For solution E, 0.27 g of ferric chloride hydrate was dissolved in 20 mL of deionized water and then mixed with 20 mL of PAA solution (3.5 wt %). The solution was then mixed with 0.1 mL of palladium chloride solution (0.01 M) and 0.5 mL of ammonia solution (28−30%, J. T. Backer). For solution F, 0.75 g of sodium borohydride was dissolved in 10 mL of deionized water. Solution F was then added to solution E dropwise under vigorous stirring. With the addition of solution F, the solution became darker, accompanied by generation of numerous bubbles. The reaction was presumed to be complete once bubble formation stopped. The final pH value of the solution was 9.50, the final Pd to Fe mole ratio was 1:1000, and the Fe to PAA weight ratio was 1:14.

The iron nanoparticles were very small (<10 nm in diameter) and were dispersed well in the solution, so they could not be separated by a magnet or centrifugation. Acetone, at a volume 5 times that of

(18) Linderoth, S. Ultrafine Amorphous Alloy Particles. *Hyperfine Interact.* **1991**, *68* (1−4), 107−118.

(19) Seip, C. T.; O'Connor, C. J. Fabrication and organization of self-assembled metallic nanoparticles formed in reverse micelles. *Nanostruct. Mater.* **1999**, *12* (1), 183.

(20) Xiaomin, N.; Xiaobo, S.; Huagui, Z.; Dongen, Z.; Dandan, Y.; Qingbiao, Z. Studies on the one-step preparation of iron nanoparticles in solution. *J. Cryst. Growth* **2005**, *275* (3−4), 548.

(21) Yang, C.; Xing, J.; Guan, Y.; Liu, J.; Liu, H. Synthesis and characterization of superparamagnetic iron nanocomposites by hydrazine reduction. *J. Alloys Compd.* **2004**, *385* (1−2), 283.

(22) Chou, K. S.; Huang, K. C. Studies on the chemical synthesis of nanosized nickel powder and its stability. *J. Nanopart. Res.* **2001**, *3* (2−3), 127−132.

(23) Hedge, M. S.; Larcher, D.; Dupont, L.; Beaudoin, B.; Tekaia-Elhsissen, K.; Tarascon, J. M. Synthesis and chemical reactivity of polyol prepared monodisperse nickel powders. *Solid State Ionics* **1996**, *93* (1−2), 33−50.

(24) Yong, K. T.; Sahoo, Y.; Choudhury, K. R.; Swihart, M. T.; Minter, J. R.; Prasad, P. N. Shape control of PbSe nanocrystals using noble metal seed particles. *Nano Lett.* **2006**, *6* (4), 709−714.

Scheme 1

$$2FeCl_3 + 6NaBH_4 + 18H_2O \rightarrow 2Fe + 21H_2 + 6B(OH)_3 + 6NaCl$$

the iron nanoparticle solution, was added. A black gel, which was composed of PAA and iron nanoparticles, was generated and separated from the solution by a strong magnet. Deionized water was then used to redisperse the black gel to obtain a well-dispersed Fe colloidal solution.

The seeding effect was also investigated. In this case, the experiment followed the same procedures mentioned above except the palladium chloride solution was not added. After reaction, a strong magnet was used to separate the iron nanoparticles. The iron nanoparticles were washed and dispersed in deionized water.

Characterization. The specific surface area of synthesized iron powder was determined by the Brunauer−Emmet−Teller (BET) method (ASAP 2000, Micromeritics). X-ray diffraction (UD-3000, Scintag) was performed to determine the composition and crystal structure. X-ray photoelectron spectroscopy (XPS; Axis 165, Kratos) was used to identify the chemical composition of the surface of iron nanoparticles. In addition, inductively coupled plasma mass spectrometry (ICP-MS; SCIEX ELAN 5000, Perkin-Elmer) was utilized to determine the composition of the powder. To estimate the content of iron oxide, thermogravimetric analyis (TGA; thermogravimetric analyzer TGA 7, Perkin-Elmer) was performed on the powder in air up to 600 °C at a heating rate of 10 °C/min. Scanning electron microscopy (SEM; S-4700I, Hitachi, Japan) and transmission electron microscopy (TEM; H-600, Hitachi, Japan, and JEM 2100F, JEOL, Japan) were used to observe the particle diameter and morphology of the nanoparticles. A rough estimate of the packing density was made by first milling each dried powder sample using a mortar and pestle, hand packing the powder into a preweighed 1 mL pipet, and weighing the pipet and powder. The magnetic properties of the iron nanoparticles were evaluated using a superconducting quantum interference device (SQUID) magnetometer (magnetic property measurement system, or MPMS, Quantum Design) at 5 and 350 K.

UV−vis spectroscopy (CARY 50 Bio, Varian) was used to determine the concentration of ferric (Fe^{3+}) ion. Standard solutions from 2.0 to 8.0 ppm were produced by mixing the following solutions: 0.4−1.6 mL of ferric chloride solution (0.0018 M), 1 mL of 3% hydrogen peroxide (original 30%, Fisher, diluted by deionized water) solution, and 5 mL of potassium thiocyanate (KSCN; 99%, Sigma) solution (2 M). The solutions were diluted with deionized water to a total volume of 20 mL. Hydrogen peroxide was used to oxidize the ferrous (Fe^{2+}) ion to form ferric (Fe^{3+}) ion. Potassium thiocyanate reacted with ferric ion to form $Fe(SCN)^{2+}$ ion, changing the color of the solution from yellow to red. The absorption of the solution at a 474 nm wavelength was measured to determine the concentration of $Fe(SCN)^{2+}$ ion.

Results and Discussion

Synthesis of Iron Nanoparticles without Dispersing Agent. In this system, the formation of iron by reaction of a ferric chloride precursor can be described according to Scheme 1.

After reaction, in the absence of any dispersing agent, iron nanoparticles quickly agglomerated and were easily separated from the solution by a strong magnet. Black powder was obtained after washing and freeze-drying. The morphology of the synthesized iron nanoparticles is shown in Figure 1a.

The specific surface area of the powder was about 36 m^2/g. From the equation

$$S = 6/\rho d \quad (1)$$

where S = specific surface area of the powder, ρ = particle density, and d = primary particle diameter, assuming the particles were pure iron and spherical, with a density of 7.97 g cm^{-3}, the number average primary particle diameter was found to be approximately 21 nm.

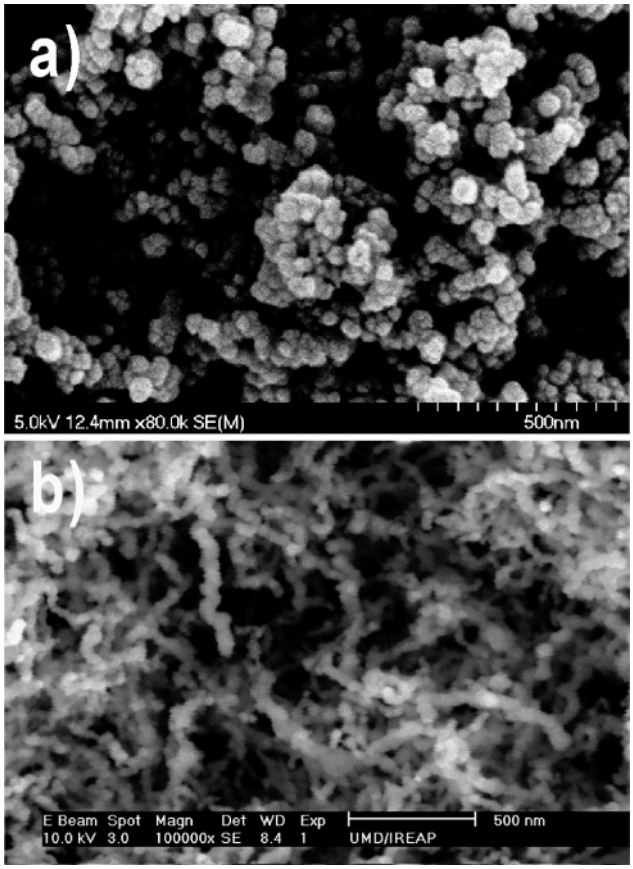

Figure 1. SEM picture of iron nanoparticles synthesized without addition of a dispersing agent: (a) without palladium seeds, magnification 80000×, (b) with palladium seeds, magnification 100000×.

The morphology of Pd-seeded iron nanoparticles is shown in Figure 1b. Like iron nanoparticles without Pd seeds, the iron nanoparticles were agglomerated. The specific surface area was about 27 m^2 g^{-1}, which is less than that without Pd seeds. Comparing the structure of the aggregates, Pd-seeded iron nanoparticle aggregates were more stringlike and the overall structure was qualitatively more porous as shown in Figure 1b. This was also apparent in packing density measurements, with the Pd-seeded particles having a packing density of 0.18 g cm^{-3}, significantly less than the packing density of 0.29 g cm^{-3} for the particles produced without seeds. Palladium is more easily reduced than iron, and thus, we hypothesize that palladium clusters were produced before the iron ion was reduced. Palladium clusters presumably acted as the seeds for heterogeneous nucleation of iron, and hence, the nucleation rate was increased in this case. The fast nucleation rate could be expected to generate a large number of particles in a short time in a small volume. Therefore, these particles likely aggregated quickly as small clusters because they were very close to each other. This quick aggregation decreased the specific surface area and led to formation of stringlike structures.

In the case of particles formed without seeds, the nuclei formed by homogeneous nucleation may have formed more slowly and may have been present at a lower number concentration at any given point in time. Thus, collisions between clusters would have been less frequent, with the particles growing mainly by condensation. We further hypothesize that, with lower concentrations of clusters, aggregation would have occurred at a later stage of particle formation, between larger and more stable or less sticky particles. These particles would be more likely to rearrange into more densely packed structures to maximize their

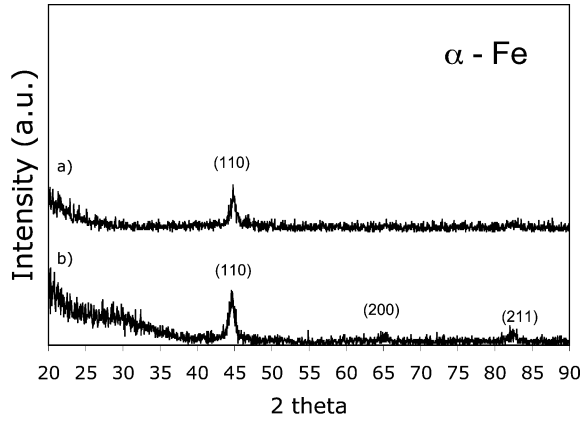

Figure 2. XRD pattern of iron nanoparticles without dispersing agent: (a) without Pd seeds, (b) with Pd seeds.

coordination number and minimize the surface free energy. This agrees with results predicted by simulations of diffusion-limited aggregation in which particles are allowed to rearrange after the initial collision, forming structures with a higher fractal dimension.[25]

Composition of Iron Nanoparticles without Dispersing Agent. Figure 2 shows the XRD patterns of iron nanoparticles synthesized without addition of a dispersing agent. The diffraction patterns indicate the nanoparticles were mainly composed of α-Fe.

The detection limit of X-ray diffraction is affected by several factors such as instrument resolution and scanning rate. Generally, it is not possible to detect the presence of other crystalline species at less than 5 wt %.[26] In addition, the peak-broadening effect characteristic of small nanoparticles could also adversely affect the detection limit. As a result, another technique was used to determine the composition of the iron nanoparticles. From ICP-MS analysis, 6 wt % boron was detected in the sample of iron nanoparticles without Pd seeds, possibly in the form of residual $B(OH)_3$ remaining after the chemical reduction reaction. Because the iron nanoparticles possessed a large specific surface area, the $B(OH)_3$ was hard to remove completely by washing.

The results of XPS analysis for the iron nanoparticles synthesized without dispersing agent are shown in Figure 3a,b. In the binding energy range of iron, only oxidized iron could be detected on the surface of the particles. However, from the XRD pattern mentioned above, no peak characteristic of iron oxide was observed. This suggests only a thin layer of iron was oxidized and most of the iron in the nanoparticles remained elemental although the particles were synthesized in an aqueous solution under ambient air, freeze-dried overnight, and then stored in air for a week prior to the XRD analysis. After etching for 300 s with electrons, the XPS analysis for iron nanosized powder with Pd seeds showed a pure iron peak as shown in Figure 3c. This result also confirmed that only the surface of the iron nanoparticles was oxidized.

To determine the degree of oxidation of the iron nanoparticles, TGA analysis was performed, and the result is shown in Figure 4. When the iron nanoparticles without Pd seeds were heated in air up to 600 °C at 10 °C min^{-1}, a significant increase in weight (33%) was observed, which was attributed to the oxidation of the iron core. By combining the result from ICP-MS and the mass balance before and after heating, and assuming complete

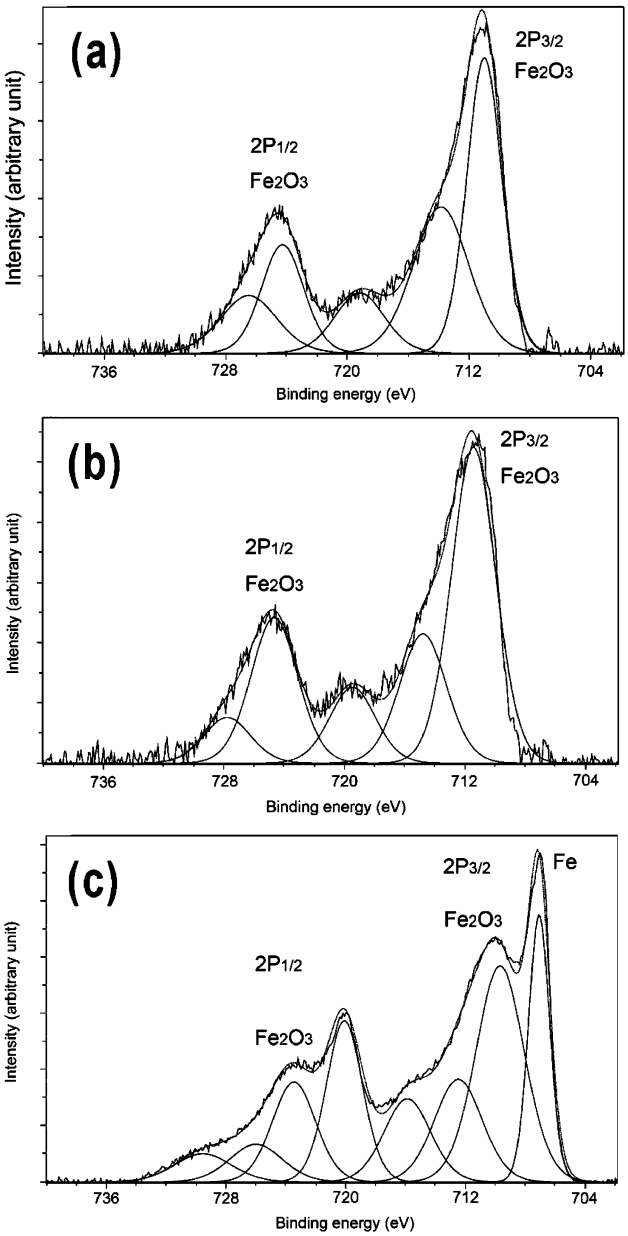

Figure 3. XPS analysis of iron nanoparticles synthesized without dispersing agent: (a) with Pd seeds, (b) without Pd seeds, (c) with Pd seeds, after etching with electrons for 300 s.

oxidation of boron, the composition of the powder can be estimated as 90.6 wt % Fe, 3.3 wt % Fe_2O_3, and 6.1 wt % B_2O_3.

Synthesis of Iron Nanoparticles with Dispersing Agent at Lower pH. Iron nanoparticles can be obtained without the dispersing agent as mentioned above. However, the nanoparticles were agglomerated and hard to redisperse even with sonication. To obtain well-dispersed iron nanoparticles, suitable dispersing agents are needed. In our work, several dispersing agents were tested including PVP, PAA, CMC, and SDS. However, as reported in detail in the Supporting Information, all of them except PAA failed to keep the iron nanoparticles from quickly agglomerating. Only PAA has carbonyl functional groups, which can adsorb on the surface of the iron nanoparticles. As a result, PAA was chosen as the dispersing agent in this work.

After reaction, the solution was a dark gray color with some large particles settling out within an hour. However, some presumably smaller particles remained suspended in solution for 8 h, indicating PAA successfully kept the particles from quick agglomeration. Most of the particles could be attracted by a

(25) Meakin, P.; Jullien, R. The Effects Of Restructuring On The Geometry Of Clusters Formed By Diffusion-Limited, Ballistic, And Reaction-Limited Cluster Cluster Aggregation. *J. Chem. Phys.* **1988**, *89* (1), 246−250.

(26) Chung, F. H.; Smith, D. K. *Industrial Applications of X-Ray Diffraction*; Marcel Dekker, Inc.: New York, 2000; pp 23−24.

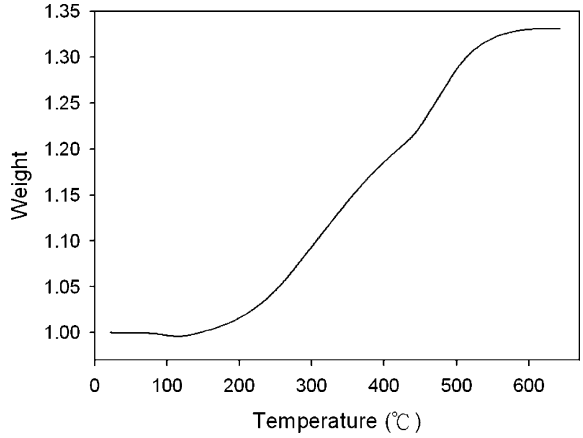

Figure 4. Weight gain as a function of temperature of iron nanoparticles without Pd seeds, measured using thermogravimetric analysis.

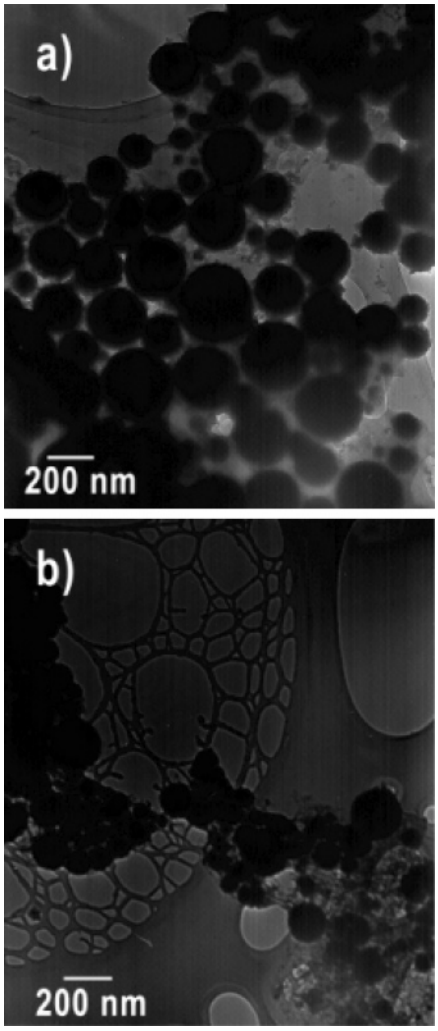

Figure 5. TEM pictures, both at 40000× magnification, of iron nanoparticles with the dispersing agent PAA at low pH: (a) without Pd seeds, (b) with Pd seeds.

strong magnet and separated from the solution. After washing and redispersion, TEM was performed to identify the morphology of iron nanoparticles, and the result is shown in Figure 5. The particle diameter distribution, obtained by measuring particle diameters from the TEM images, is shown in Figure 6. A log-normal distribution was fit to the measured diameter distribution of the iron nanoparticles, and this is shown as the solid line in Figure 6.

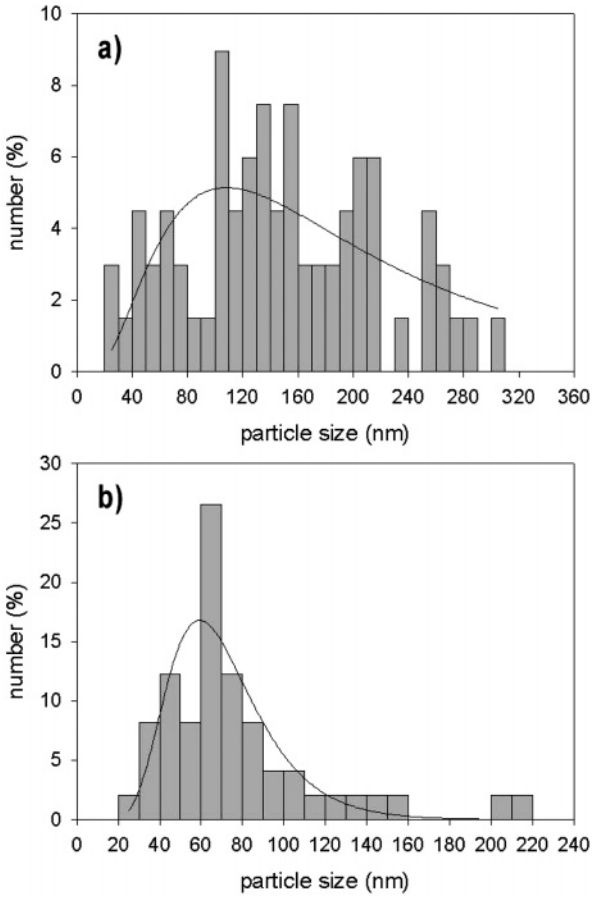

Figure 6. Particle diameter distribution of iron nanoparticles with the dispersing agent PAA at low pH: (a) without Pd seeds, (b) with Pd seeds. The line indicates a log-normal fit to the diameter distribution.

Figure 5 shows iron particles were spherical and not strongly necked regardless of whether or not palladium seeds were added. However, the particles synthesized with palladium seeds were smaller, with a geometric mean diameter of 59 nm versus 110 nm for particles synthesized without seeds. Furthermore, particles with palladium seeds were more monodisperse in size, as shown in Figure 6b, with a geometric standard deviation of 1.4 versus 2.0 for particles synthesized without seeds. In the absence of palladium seeds, as described previously, the nucleation rate is likely lower, and this would lead to a greater distribution of particle residence times and thus a greater range of particle diameters, as particles nucleating first grow large, while those formed later in the synthesis are smaller. The reduction in particle diameter seen for particles synthesized with seeds is also explained by the action of the seeds, leading to a higher concentration of initial nuclei. A similar reduction in particle size with addition of noble metal seeds was observed for the thermal decomposition synthesis of nickel nanoparticles with silver[27] and palladium seeds.[23]

Figure 7 shows PAA was adsorbed on the surface of iron nanoparticles prepared with Pd seeds at pH 8.75 to keep them from aggregating. The thickness of this PAA film is about 3 nm regardless of the particle diameter. Hence, with decreasing iron nanoparticle diameter, the volume of residual PAA increases, even after washing to remove the free PAA. The minimum volume of residual adsorbed PAA can be estimated using the following

(27) Fievet, F.; Lagier, J. P.; Blin, B.; Beaudoin, B.; Figlarz, M. Homogeneous and heterogeneous nucleations in the polyol process for the preparation of micron and submicron size metal particles. *Solid State Ionics* **1989**, *32*−33 (Part 1), 198.

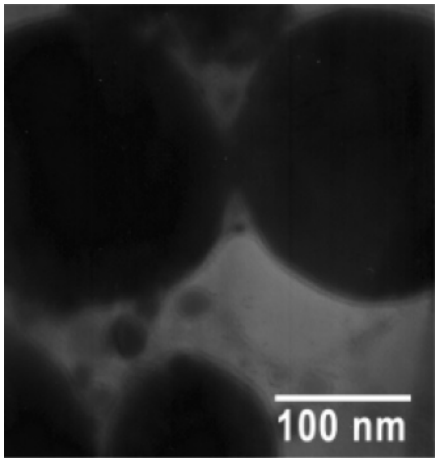

Figure 7. TEM image, at a magnification of 230000×, of PAA adsorbed on the surface of iron nanoparticles. The thickness of the adsorbed PAA layer is about 3 nm.

equation:

$$V_{PAA} = 6\alpha/\rho d \qquad (2)$$

where V_{PAA} represents the specific volume of PAA adsorbed per unit weight of iron nanoparticles, α (3 nm) represents the thickness of the PAA film, d represents the diameter of the iron nanoparticles, and ρ (7.97 g/cm^3) represents the density of iron. For 200 nm diameter particles, we estimate only 0.01 cm^3 of PAA is adsorbed on 1 g of iron nanoparticles. This relative amount of adsorbed PAA increases to 0.11 cm^3 when the particle diameter decreases to 20 nm. Assuming a PAA density of 1 g cm^{-3}, and converting to a PAA:Fe weight ratio, for the case of 20 nm diameter nanoparticles, this weight ratio is approximately 1:9. By comparison with the initial PAA:Fe weight ratio of 14:1, we see that most of the PAA is removed in the washing step.

As mentioned above, the addition of palladium can increase the number of nuclei and subsequently decrease the diameter of iron nanoparticles. In addition, in the reaction with Pd seeds, less $NaBH_4$ solution was required before the solution turned black. This suggests that iron nanoparticles were generated faster. Although the same quantity of sodium borohydride was added in the end, the solution with Pd seeds turned completely dark when only about one-third of the amount of $NaBH_4$ was added. However, in the reaction without Pd seeds, the solution did not turn completely dark until most of the $NaBH_4$ solution had been added. This is because without Pd seeds the iron nanoparticles were formed via homogeneous nucleation, and therefore, a higher supersaturation was required before iron nanoparticles were produced.

Synthesis of Iron Nanoparticles with Dispersing Agent at Higher pH and Addition of Pd Seeds. For the reaction with Pd seeds, after washing and redispersion, a black iron nanoparticle colloidal solution was obtained. The morphology of the iron nanoparticles and particle diameter distribution are shown in Figure 8. The iron nanoparticles were found to be smaller than 10 nm, and the particle diameter distribution was very uniform. Compared to an electron diffraction pattern reported for iron nanoparticles in the literature,[10] the iron nanoparticles here appear to contain only crystalline iron. The geometric mean diameter was 6 nm, and the geometric standard deviation was 1.3.

The iron nanoparticle colloidal solution was well dispersed, and no precipitate was found after 2 weeks; however, a large amount of PAA inevitably existed. To determine the ratio of Fe to PAA of the particles shown in Figure 8, the dry iron

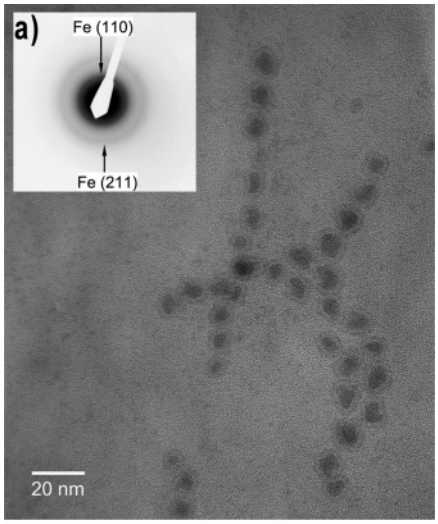

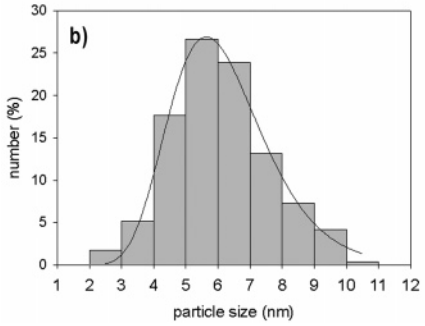

Figure 8. (a) TEM image of iron nanoparticles, at a magnification of 400000×, synthesized with the dispersing agent PAA and Pd seeds at a pH of 9.50. (b) Particle diameter distribution of the iron nanoparticle colloidal solution. The line indicates a log-normal fit to the diameter distribution.

nanoparticles were dissolved in hydrochloric acid solution and reacted with SCN^- ion to form an $Fe(SCN)^{2+}$ complex. Hydrogen peroxide solution was used to oxidize any existing ferrous ion to ferric ion. UV−vis spectroscopy was used to determine the concentration of $Fe(SCN)^{2+}$ by measuring the absorption at 474 nm. The mass ratio of PAA to Fe in the iron nanoparticle colloidal solution was determined as 17:1. This is similar to the starting ratio of 14:1 and suggests that the PAA and iron nanoparticles were both precipitated out of solution using acetone with approximately the same efficiency. Using eq 2, the specific adsorbed volume of PAA, as visible in the TEM image in Figure 8, was estimated to be 0.38 g cm^{-3} of iron, assuming a 3 nm thick coating of PAA. This gives a PAA to Fe mass ratio of 1:2.6, suggesting that, in this case also, there was a large amount of unadsorbed PAA remaining in solution.

Without Pd Seeds. For the reaction without Pd seeds, after washing and redispersion, the morphology of iron nanoparticles and particle diameter distribution are shown in Figure 9. The geometric mean diameter was 110 nm, and the geometric standard deviation was 1.5. The particle size is the same as in the case of low pH, and no Pd seeds, but as described below, the high pH likely increases ionization of PAA, increasing its dispersing capability and reducing the polydispersity.

Effects of Pd Seeds and pH on the Diameter of Iron Nanoparticles. The statistics describing the diameter distribution of iron nanoparticles generated by different synthesis processes are summarized in Table 1. The diameter distribution can be explained by the theory of nucleation and growth mechanism as shown in Figure 10. Without Pd seeds, the synthesis of iron nanoparticles followed a homogeneous nucleation mechanism

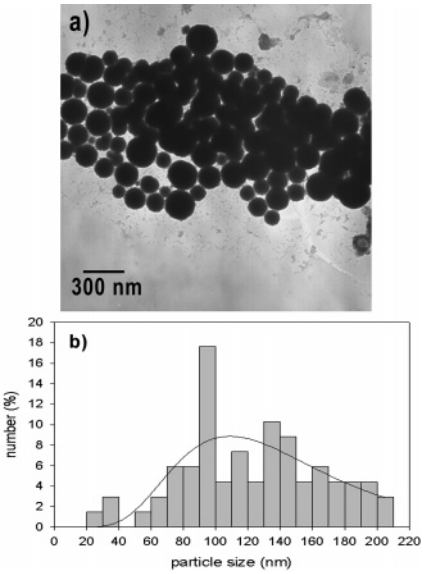

Figure 9. (a) TEM image, at a magnification of 33000×, of iron nanoparticles with dispersing agent at higher pH without Pd seeds. (b) Diameter distribution of iron nanoparticles with dispersing agent at higher pH without Pd seeds. The line indicates a log-normal fit to the particle diameter distribution.

Table 1. Summary of Statistics for the Diameter of Iron Nanoparticles[a]

seed conditions	low pH	high pH
without Pd seeds	$D_g = 110$ nm $\sigma_g = 2.0$	$D_g = 110$ nm $\sigma_g = 1.5$
with Pd seeds	$D_g = 59$ nm $\sigma_g = 1.4$	$D_g = 6$ nm $\sigma_g = 1.3$

[a] D_g is the geometric mean diameter, and σ_g is the geometric standard deviation.

and higher supersaturation was required. As a result, less iron nuclei were produced, and subsequently, only large iron nanoparticles, with a wide distribution in particle diameters, were obtained. On the contrary, with Pd seeds, the synthesis of iron nanoparticles followed a heterogeneous nucleation mechanism because there were many Pd nuclei produced in the solution before iron was reduced. Therefore, small or medium iron nanoparticles were obtained.

In addition to Pd seeds, the conformation of PAA chains at different pH values also has a great effect on the particle diameter distribution of iron nanoparticles. PAA, as a water-soluble polymer, can ionize in the water and release protons. At lower pH (8.75), less PAA can ionize, so PAA chains shrink and the ability to prevent Pd seeds from agglomerating is reduced. As a result, the Pd seeds were easily agglomerated and the number of nuclei decreased. Therefore, medium-sized iron nanoparticles were obtained. On the contrary, at higher pH (9.50) more PAA is ionized. Because of the electrostatic repulsion, the PAA chains are more elongated, and consequently, their ability to disperse particles increases. As a result, the Pd seeds can be dispersed well, and subsequently, small iron nanoparticles were obtained because of the larger amount of nuclei.

The magnetic properties of iron nanoparticles produced at high pH (9.50) with PAA were also measured using a SQUID magnetometer, and the result is shown in Figure 11. From the magnetization hysteresis loop at 5 K, the saturation magnetization is about 120 emu g^{-1}. In addition, from the magnetization behavior at 350 K the sample became superparamagnetic because of thermal agitation, another result of the small diameter of iron

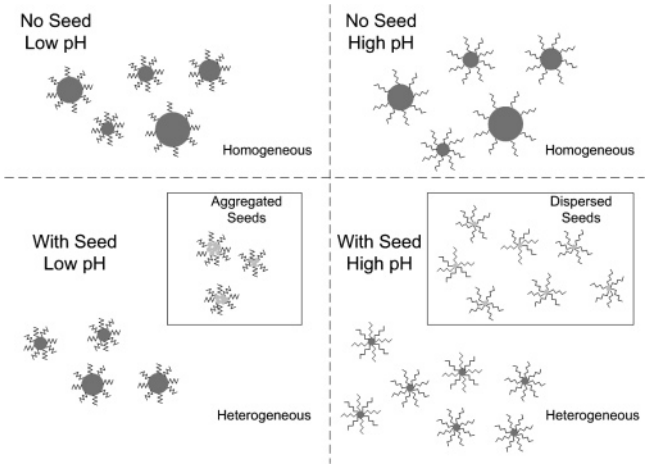

Figure 10. Schematic illustration of the nucleation and growth mechanism of iron nanoparticles.

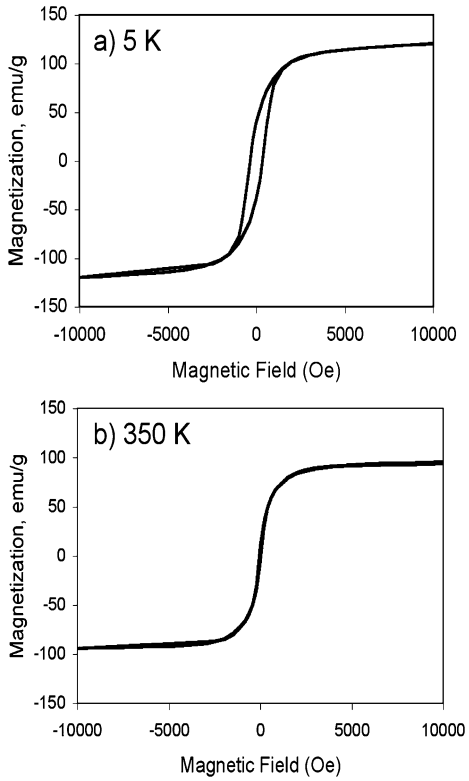

Figure 11. Magnetization hysteresis loops of iron nanoparticles, 6 nm in diameter, measured at (a) 5 K and (b) 350 K.

nanoparticles. The saturation magnetization value is much less than that for bulk iron, 222 emu g^{-1} at 298 K.[28] However, our results are comparable to values of saturation magnetization reported previously for iron nanoparticles in this size range, for example, 82 emu g^{-1},[29] 175 emu g^{-1},[10] and 190 emu g^{-1},[30] for 6, 7, and 20 nm diameter iron nanoparticles, respectively. Iron nanoparticles produced without dispersing agent and without Pd seeds were also characterized using SQUID, and the particles

(28) Cullity, B. D. *Introduction to Magnetic Materials*; Addison-Wiley: New York, 1972; pp 171−190.
(29) Griffiths, C. H.; Ohoro, M. P.; Smith, T. W. Structure, Magnetic Characterization, And Oxidation Of Colloidal Iron Dispersions. *J. Appl. Phys.* **1979**, *50* (11), 7108−7115.
(30) Gangopadhyay, S.; Hadjipanayis, G. C.; Dale, B.; Sorensen, C. M.; Klabunde, K. J.; Papaefthymiou, V.; Kostikas, A. Magnetic-Properties Of Ultrafine Iron Particles. *Phys. Rev. B* **1992**, *45* (17), 9778−9787.

were found to be ferromagnetic at both 5 and 350 K. Further details are given in the Supporting Information.

Conclusions

Iron nanoparticles with a large surface area were synthesized from $FeCl_3 \cdot 6H_2O$ by $NaBH_4$ as the reducing agent in the absence of a dispersing agent. X-ray diffraction results indicated the iron nanoparticles were composed of α-Fe. XPS and TGA analyses showed the surface of iron nanoparticles was oxidized, with the particles containing about 3 wt % iron oxide. SEM pictures showed palladium acted as seeds and affected the morphology of the iron nanoparticles. Addition of palladium likely leads to loosely packed iron nanoparticles, because of the increase in nucleation rate and subsequent stringlike aggregation of the nanoparticles.

Using PAA as the dispersing agent, aggregation of iron nanoparticles was prevented. Stringlike aggregation could be prevented in the reaction without Pd seeds because of the presence of the dispersing agent PAA. However, the geometric mean diameter of iron nanoparticles was larger than 100 nm. The synthesis occurred via homogeneous nucleation, and only a few iron nuclei were produced as the seeds for iron nanoparticles.

In the reaction with Pd seeds and dispersing agent, the diameter of the iron nanoparticles was noticeably less. In the higher pH solution, pH 9.50, relatively monodisperse α-Fe nanoparticles of about 6 nm were obtained. These nanoparticles were easily redispersed in deionized water to form a colloidal iron solution with long-term stability. The iron nanoparticles are superparamagnetic at 350 K, a result expected on the basis of their small diameter. However, at lower pH (8.75) the dispersing capability of PAA was reduced, and consequently, the number of Pd seeds likely decreased because of agglomeration. Therefore, iron nanoparticles about 59 nm in geometric mean diameter were obtained.

In summary, iron nanoparticles with different diameters and morphologies can be synthesized by controlling the addition of dispersing agent and Pd seeds and by adjusting the pH value of the solution. This synthesis route is considered an economical and convenient method to fabricate iron nanoparticles suitable for various applications such as MRI contrast enhancement, bioseparations, Ni−Fe batteries, and catalysts for carbon nanotube growth.

Acknowledgment. We thank Ichiro Takeuchi and Makoto Murakami for assistance with magnetic characterization, Ranjan Pati for assistance with high-resolution TEM, and Bindu Varughese for assistance with XPS. Support from the National Science Foundation under Grant No. DMR-0080008 for the purchase of the XPS instrument is acknowledged. This material is based upon work supported partially by the National Science Foundation under Grant No. NSF-MRSEC-DMR-0080008. K.-C.H. also thanks the National Science Council of Taiwan for partial financial support under Grant No. NSC 094-2917-I-007-008.

Supporting Information Available: Results for additional dispersing agents and additional magnetic property characterization. This material is available free of charge via the Internet at http://pubs.acs.org.

LA0618364